Naval Research Laboratory
Washington, DC 20375-5000

NRL Memorandum Report 6675

NRL Beam Propagation Theory Studies in Support of SuperIBEX, PULSERAD, RADLAC, PURE and DELPHI

R. F. HUBBARD, A. W. ALI, P. BORIS,* R. F. FERNSLER, G. JOYCE, M. LAMPE, S. P. SLINKER AND R. D. TAYLOR**

Beam Physics Branch
Plasma Physics Division

**Science Applications International Corp.*
McLean, VA 22102

***Berkeley Research Associates*
Springfield, VA 22150

August 31, 1990

REPORT DOCUMENTATION PAGE

Form Approved
OMB No. 0704-0188

1. AGENCY USE ONLY (Leave blank)	2. REPORT DATE	3. REPORT TYPE AND DATES COVERED
	1990 August 31	Interim

4. TITLE AND SUBTITLE
NRL Beam Propagation Theory Studies in Support of SuperIBEX, PULSERAD, RADLAC, PURE and DELPHI

5. FUNDING NUMBERS
JO #47-0900-0-0

ARPA Order #4395, A86

6. AUTHOR(S)
R. F. Hubbard, A. W. Ali, P. Boris,* R. F. Fernsler, G. Joyce, M. Lampe, S. P. Slinker and R. D. Taylor**

7. PERFORMING ORGANIZATION NAME(S) AND ADDRESS(ES)
Naval Research Laboratory
Washington, DC 20375-5000

8. PERFORMING ORGANIZATION REPORT NUMBER
NRL Memorandum Report 6675

9. SPONSORING/MONITORING AGENCY NAME(S) AND ADDRESS(ES)
DARPA
Arlington, VA 22209

NSWC
Silver Spring, MD 20903-5000

10. SPONSORING/MONITORING AGENCY REPORT NUMBER

11. SUPPLEMENTARY NOTES
*Science Applications International Corp., McLean, VA 222102
**Berkeley Research Accociates, Springfield, VA 22150

12a. DISTRIBUTION/AVAILABILITY STATEMENT
Approved for public release; distribution unlimited.

12b. DISTRIBUTION CODE

13. ABSTRACT (Maximum 200 words)

NRL beam propagation studies in support of SuperIBEX, PULSERAD, and RADLAC experiments and theoretical studies concerning the PURE and DELPHI concepts are summarized in a series of short papers which were presented at the 1989 Annual DARPA/SDIO/Services Charged Particle Beam Review. The first of these papers contains an overview of beam propagation in reduced-density channels. The second describes simulation studies of past and future channel tracking experiments on NRL's SuperIBEX and PULSERAD devices. The effect of the frequency spectrum of initial perturbations on the hose instability is described in the next paper. The fourth paper investigates the feasibility of using near-term experiments to simulate the physics of pulse decoupling in long-range propagation. The next paper describes electron energy deposition in O^+, expected to be a major constituent of a PURE mode channel. Analytical and simulation studies of the virulent transverse two-stream instability, a potential problem for the PURE and DELPHI propagation concepts, are described in the last paper.

14. SUBJECT TERMS
channel tracking
ion-focused regime
hose instability
beam propagation
charged particle beams
air chemistry

15. NUMBER OF PAGES
41

16. PRICE CODE

17. SECURITY CLASSIFICATION OF REPORT	18. SECURITY CLASSIFICATION OF THIS PAGE	19. SECURITY CLASSIFICATION OF ABSTRACT	20. LIMITATION OF ABSTRACT
Unclassified	Unclassified	Unclassified	SAR

CONTENTS

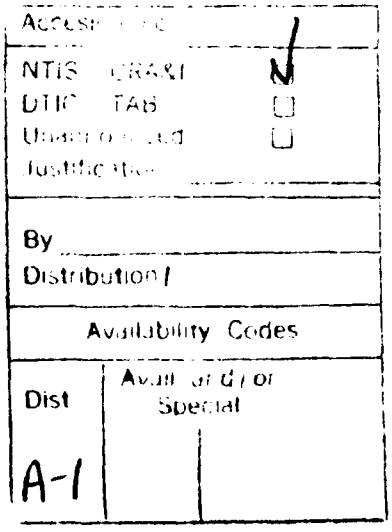

NRL BEAM PROPAGATION THEORY STUDIES IN SUPPORT OF SUPERIBEX, PULSERAD, RADLAC, PURE AND DELPHI

OVERVIEW

This report contains six short papers which will appear in the Proceedings of the Annual DARPA/SDIO/Services Charged Particle Beam Review which took place at the Naval Postgraduate School in Monterey, CA during 18-21 September, 1989. The papers describe electron beam propagation studies which have been carried out at NRL in support of beam propagation experiments at several laboratories.

Most of these experiments involve high current propagation in air. In some cases, the beam range is extended by propagating the beam in a reduced-density channel. SuperIBEX is a new 5 MeV, 10-40 kA device located at NRL which will be used for both beam stability and channel tracking studies. PULSERAD is an older 1 MeV, 10 kA diode at NRL which in 1987 performed the first successful channel tracking experiments. RADLAC is an induction accelerator located at Sandia National Laboratories which is expected to produce up to 40 kA at an energy of 20 MeV. PURE is an entirely different propagation concept which would use an RF linac to produce a train of micron-sized beam pulses at lower current but very high energy. DELPHI is a high altitude beam propagation concept currently being developed at Sandia which would employ laser-ion guiding to propagate an electron beam in a diffuse plasma.

Some of the papers included here also describe predictions for the ATA Multi-Pulse Propagation Experiment (MPPE) which was recently completed at Lawrence Livermore National Laboratory. NRL papers in the Annual Propagation Review which were devoted solely to that experiment are included in a separate report.

A brief summary of each paper and a list of co-authors for those papers are given below.

A. Beam Propagation in Channels: This paper contains an overview of NRL research on propagation in channels and provides a brief summary of most of the papers described below in this section of the quarterly report. Most of the work has been in support of the ATA Multi-Pulse Propagation Experiment (MPPE). Included are hose instability simulations, detailed air chemistry and channel physics calculations of ATA/MPPE. Simulation studies

Manuscript approved May 21, 1990.

of SuperIBEX, PULSERAD and RADLAC propagation experiments are also discussed. (Hubbard, Slinker, Taylor, Fernsler, Ali, Joyce, Boris)

B. Analysis of Channel Tracking in SuperIBEX and PULSERAD: SARLAC was used to simulate both the 1988 PULSERAD tracking experiment and the upcoming Super-IBEX experiment. Expected trends were found; for example, higher beam currents resulted in increased hose motion (shorter e-folding distances) as well as stronger tracking forces (shorter tracking distances). Other interesting results emerged from the studies as well. First, the general features of the PULSERAD experiments were reproduced. In particular, beam deflections and tracking distances were consistent with the observations. The hose e-folding distances were comparable to the tracking distances. Also, the channel had little apparent effect on the hose instability. While there was an apparent increase in hose growth in the presence of a channel, this effect was primarily due to the reduction in scattering; the effect disappeared when the results were properly scaled to the number of betatron wavelengths propagated by the beam. Second, Super-IBEX simulations showed that beam deflections and tracking distances should be measurable, with characteristic hose distances being much longer than tracking distances. That is, with projected initial (low frequency) perturbations, the channel may stabilize hose. This last effect is, in part, a consequence of the choice of the initial perturbation on the beam, which does not couple to the hose instability as strongly as a high frequency perturbation (PULSERAD). The stabilization also may result from higher return currents flowing at the edge of the channel. These simulations demonstrate the importance of limiting high frequency perturbations in stability and tracking experiments. Similar predictions regarding the importance of initial beam perturbation to subsequent stability properties have been made with regard to the ATA/MPPE and RADLAC. (Taylor, Fernsler, Hubbard, Slinker)

C. Sensitivity of Hose Instability to Frequency of Initial Perturbations in Low and High Current Beams: Increases in the solenoidal guide field B_z used in the ATA accelerator tend to reduce the growth of high-frequency BBU growth in the accelerator but enhance the generation of low-frequency sweep within the pulse. Hose instability in the propagating beam arises from initial perturbations generated by BBU and/or sweep. To examine the trade-offs between these two effects, a series of SARLAC simulations of ATA/MPPE were performed with an 830 MHz BBU-like perturbation in the x-direction and a simple linear sweep in the y-direction. The

relative amplitudes of these perturbations were estimated from analytical models. In all cases, the BBU-like perturbations grew more rapidly as the beam propagated in air and eventually dominated even when suppressed by a 3 kilogauss guide field. One encouraging result was that sweep amplitudes much larger than the 0.01 cm design target for ATA/MPPE could apparently be tolerated. The results strongly suggest that suppression of BBU growth will be an important operational consideration. Similar simulations were carried out for the higher current RADLAC parameter regime; these simulations also showed that high frequency perturbations were more dangerous. One should be aware that high frequency perturbations within the beam lead to low frequency oscillations in z because the perturbations couple to hose in the beam head where the dipole decay length is short but the betatron wavelength is long. (Hubbard, Slinker, Taylor)

D. Pulse Decoupling Using ATA: The channel created by a multi-pulse CPB burst becomes broader and shallower as the beam propagates. Eventually, the channel tracking force becomes too weak to guide the pulse, and the geomagnetic field deflects the beam out of the channel. ATA can in principle be used to simulate this complicated process experimentally. One possible strategy would be to create a channel with four pulses and apply a weak deflecting magnetic field to the fifth pulse. SARLAC simulations, however, suggest that wall forces in the ATA propagation tank would tend to obscure the result, and the propagation distance required to observe the effect is relatively long. It may be easier to study pulse decoupling with the laser-guided discharge channels used with SuperIBEX since the tracking forces are expected to be much stronger, the channel depth is independent of z, and the wall radius is much larger, (Fernsler, Slinker, Hubbard)

E. Electron Energy deposition in O^+. A discrete, time-dependent energy deposition model was used to study high-energy electron-beam (100 eV to 10 MeV) deposition in O^+. O^+ is expected to be a major constituent in the hot plasma channels created by a PURE-mode pulse train. Secondary electron distributions were obtained by solving a time-dependent, relativistic Boltzmann equation. These distributions relax (nonuniformly) to steady-state results from which yield spectra, production efficiencies of specific states, energy partitioning, and mean energies per electron-ion pair production (W) were computed. Loss functions were calculated and shown to be in close agreement with Bethe's relativistic equation for energies greater than 1 keV. The model predicts W is approximately 72 eV for O^+ over

a wide range of beam energies and background ionization fractions. The effects of inner shell ionization and excitation were included in the deposition model. These effects result in an increase in W of approximately 17% for energies above 10 keV; this is a direct consequence of the increased ionization energy. While the present study, in general, has focused on beam sources, W was observed to change for energies below 1 keV if the source electrons were assumed to be completely stopped by the medium. (Taylor, Ali, Slinker)

F. Transverse Two-Stream Instability: An intense relativistic electron beam propagating through a diffuse plasma is subject to a transverse two-stream instability. Analytical dispersion relations have been derived assuming an electrostatic-magnetostatic approximation and spread-mass beam dynamics. If a Bennett-shaped IFR channel is present, (the situation expected for a DELPHI beam), the instability is hose-like and convective, and modest growth is predicted. However, if the diffuse plasma density is constant, as expected for a mature PURE channel, the dispersion relation predicts absolute instability and rapid growth. Simulations using the new 3-D ELBA particle code are consistent with the analytical model and exhibit rapid instability growth and beam disruption for the case with a constant plasma density. (Joyce, Lampe)

BEAM PROPAGATION IN CHANNELS*

R. F. Hubbard, S. P. Slinker, R. D. Taylor,** R. F. Fernsler
A. W. Ali, G. Joyce and P. Boris***
Plasma Physics Division, Naval Research Laboratory, Washington, DC 20375

I. INTRODUCTION

Beam propagation in density channels is a major focus of the current DARPA experimental program. The ATA Multi-Pulse Propagation Experiment (MPPE) will attempt to demonstrate stability, tracking, and range extension in the channel formed by a five-pulse burst of 10 MeV, 6-8 kA beams. Also, tracking experiments at NRL using the PULSERAD and SuperIBEX beams in laser-guided electric discharge (LGED) channels are in progress. This paper provides an overview of theoretical work at NRL in support of these propagation experiments. More detail can be found in Refs. 1-7.

II. ATA MULTI-PULSE PROPAGATION STUDIES

Overview: Detailed predictions for an ATA/MPPE burst require treatment of the complicated coupling between beam propagation and channel physics over times scales up to 5 msec. To address these problems, we have carried out five-pulse axisymmetric simulations which combine existing NRL propagation and channel physics codes.[1] The results are used to predict the range of each pulse and to provide realistic channels for SARLAC hose stability simulations. Supporting these simulations are more detailed studies of air chemistry effects[2] and convective cooling.[3] We have also studied the sensitivity of lead pulse hose instability growth to the amplitude of BBU and corkscrew-induced perturbations[4] and choice of emittance tailoring method.[5] We have assessed the feasibility of an ATA pulse-decoupling experiment.[6]

Typical parameters for these studies are beam energy E_0 = 10 MeV, peak current I_0 = 6 kA, nominal beam radius a_b = 0.5 cm, pulse length τ_p = 33 nsec, pulse separation τ_s = 1.25 msec, and an emittance variation of 4:1.

Multi-pulse axisymmetric propagation and channel dynamics:[1] In these simulations, the SIMMO particle code is used for $\tau < \tau_p$ to propagate the beam and dump beam current density $J_b(r,\zeta,z)$. Here, ζ is the distance from the

beam head, z is the propagation distance, and $\zeta = c\tau = ct - z$. CHMAIR II uses the J_b input from SIMMO to calculate beam and ohmic deposition and detailed air chemistry for $\tau_p < \tau < 2\tau_p$ at several z-locations. HINT is then used to calculate the long-time-scale behavior of the channel ($\tau < \tau_s$), including the effects of hydrodynamic expansion, thermal and convective cooling, and vibrational relaxation. This generates a density profile, $\rho(r,z)$, which is input into SIMMO for the next pulse in the burst, and the process is repeated.

Six simulations were run to determine the sensitivity of the channel depth and the transported beam fluence to model assumptions. The fluence, $Q_n(R,z)$, is defined as the transported beam charge for the n^{th} pulse within a radius, R, of the beam axis at a fixed location z. The ratio Q_5/Q_1 for R = 1.1 cm and z = 6 m varied between 1.4 and 1.85, indicating modest range extension. The channel depth at z = 0 was very sensitive to the assumed Picone-Boris form factor f for convective cooling;[3,8] the on-axis density at the fifth pulse was a factor of two higher when f was raised from 0 to 0.05. However, the predicted fluence at z = 6 m changed by less than 15% because the convectively-cooled channel was significantly broader. Changes in the assumed chemistry model for SIMMO and the inclusion of enhanced vibrational cooling from CO_2 produced only modest changes in the fluence.[2]

Chemistry effects and convective cooling in ATA/MPPE: A new chemistry model for SIMMO and SARLAC was developed using these same basic approach as in the standard "VIPER" model. The new model[2] includes attachment and revised rate coeficients benchmarked against detailed CHMAIR II calculations in the ATA/MPPE regime. The new model gives similar axisymmetric behavior and generates slightly more hose instability growth. The second major focus of the air chemistry studies was a treatment of the transfer of the energy stored in N_2 vibrational excitations to gas heating. This process occurs on the millisecond time scale but can be speeded up by adding a small amount of CO_2.

The Picone-Boris[8] convective cooling form factor, which we and others have used in MPPE hydro simulations is a phenomenological model which has not been benchmarked against full 2-D hydro code results in the appropriate parameter regime. A new 2-D hydro code that treats the convective cooling process directly has been developed.[3] The code runs on NRL's massively-parallel Connection Machine and is much faster than the version used by Picone and Boris. Preliminary results suggest that the value f = 0.05 used in the HINT code is reasonable for the level of asymmetry expected for ATA/MPPE.

Hose instability growth in MPPE: SARLAC simulations[1] have been carried out in the channels generated by the SIMMO-CHMAIR-HINT simulation sequence described above. Hose amplitudes in the beam body grow from an assumed initial level of 0.01 cm to 0.5-0.7 cm in 6 m of propagation. Similar hose amplitudes were observed in the absence of a channel.

Increasing the guide field B_z in ATA increases low frequency sweep displacements but suppresses high frequency BBU-induced perturbations.[4] The effect of this tradeoff on hose instability was investigated using SARLAC by initiating a BBU-like mode in x and a linear sweep in y. The BBU-induced mode was much more unstable in the simulations, while relatively large sweep amplitudes could be tolerated. In one set of SARLAC runs, increasing B_z from 1 to 3 kG caused hose amplitudes at z = 6 m to drop by almost a factor of 3.

Other SARLAC simulations considered the effects of different possible emittance tailoring techniques.[5] Beam radius and emittance profiles were generated by FRIEZR for various tailoring schemes, and the results were used to initialize SARLAC. A multi-foil tailoring cell simulation produced hose amplitudes in excess of 1 cm in 4.8 m of propagation, while a similar run using a 5 mtorr IFR cell grew to only 0.1 cm.

Pulse decoupling experiment for ATA:[6] SARLAC was used to investigate the feasibility of studying pulse decoupling experimentally on ATA by applying a weak deflecting guide field just before the last pulse. The simulation results suggest that the phenomenon would likely be obscured by wall forces.

Summary: The ATA/MPPE beams are likely to propagate with only moderate hose growth if the stringent beam conditioning goals are met. Range extension effects should be modest but observable.

III. SUPERIBEX AND PULSERAD TRACKING STUDIES

PULSERAD stability and tracking simulations:[7] A data base now exists for the 1988 NRL tracking experiments which used the 1 MeV PULSERAD beam. SARLAC simulations were performed with a weakly-tailored beam with the estimated experimental parameters. The hose amplitudes were somewhat higher in a centered density channel than in full density air, but the difference could be attributed entirely to scattering effects. Increasing I_0 appeared to destabilize the beam. The tracking distance was typically 30 cm. All of these results are consistent with the experimental data.

SuperIBEX stability and tracking simulations: SARLAC was used[7] to model the 4.5 MeV SuperIBEX tracking experiments currently in progress. The simulations assumed moderate emittance tailoring and relatively large amplitude, but low frequency initial hose perturbations. Peak simulation beam currents varied between 10 and 40 kA. Hose amplitudes increased with I_0 and were smaller in the presence of a channel than in full density air, in contrast to the PULSERAD result. Tracking distances were predicted to be only 20-30 cm in the presence of an offset channel.

A separate series of SARLAC simulations modeled propagation in a 10 m long tank in uniform 0.5 atm air and in a centered, 0.1 atm density channel. The beam was well-conditioned, as might be produced by a two-stage IFR/active-wire conditioning cell currently being considered for future experiments. The perturbations were the same as used in the RADLAC simulations described in Ref. 4. Hose amplitudes grew to only 0.2-0.3 cm in the SuperIBEX simulations.

Summary: PULSERAD simulation results were consistent with the data from the successful 1988 tracking experiment. Simulations of the current SuperIBEX tracking experiment predict short tracking distances and moderately-strong hose growth. Future SuperIBEX experiments with well-conditioned beams could exhibit "stable" propagation to ranges beyond 10 m.

IV. REFERENCES

1. S. Slinker et al., "Beam Stability and Range Extension Predictions for the ATA Multi-Pulse Experiment," these proceedings.
2. S. Slinker et al., "Air Chemistry Aspects of the ATA Multi-Pulse Experiment," these proceedings.
3. P. Boris et al., "Hydrodynamic Simulations of Beam-Generated Turbulence in Channels," these proceedings.
4. R. Hubbard et al., "Sensitivity of Hose Instability to Frequency of Initial Perturbations in Low and High Current Beams," these proceedings.
5. R. Hubbard et al., "Beam Conditioning Options for the ATA Multi-Pulse Experiment," these proceedings.
6. R. Fernsler et al., "Pulse Decoupling Using ATA," these proceedings.
7. R. Taylor et al., "Analysis of Channel Tracking in SuperIBEX and PULSERAD," these proceedings.
8. J. Picone and J. Boris, Phys. Fluids **26**, 365 (1983).

*Supported by the Defense Advanced research Projects Agency, ARPA Order No. 4395, Amendment 80, Monitored by the Naval Surface Warfare Center,

**Berkeley Research Associates, Springfield, VA 22150

***Science Applications International Corp., McLean, VA 22102

Analysis of Channel Tracking in Super-IBEX and PULSERAD*

R.D. Taylor,** R.F. Fernsler, R.F. Hubbard, and S.P. Slinker
Beam Physics Branch, Plasma Physics Division
Naval Research Laboratory, Washington, D.C. 20375

SARLAC is used to simulate both the 1988 PULSERAD tracking experiment and the upcoming Super-IBEX experiment. From a theoretical (and simulation) perspective, key questions about these experiments include: Do the simulations predict a tracking force and, if so, on a scale that is observable? Does the existence of a channel affect the stability properties of the propagating beam? Several interesting results emerge from these studies. First, the general features of the PULSERAD experiments are reproduced. In particular, beam deflections and tracking distances are consistent with the observations. Also, the channel has little apparent effect on the hose instability. Second, Super-IBEX simulations show that beam deflections and tracking distances should be measurable. In addition, with projected initial (low frequency) perturbations, the channel may stabilize hose. This last effect is, in part, a consequence of the choice of the initial perturbation on the beam. Similar predictions regarding the importance of initial beam perturbation to subsequent stability properties have been made elsewhere.[1]

The PULSERAD simulations assume a weakly tailored (1.2:1.0 over 8 ns), 1 MeV beam having: 1) a 40 ns triangular temporal profile with a 20 ns risetime and 20 ns falltime; 2) a nominal radius of 2.0 cm; 3) a variable frequency (420 MHz at the head to 102 MHz at the tail) initial hose perturbation with a 2 mm amplitude; and 4) currents of 7 and 10 kA. The channel characteristics are: 1) a minimum density equal to 0.1 times that of ambient air (ρ_o); 2) a 4.0 cm radius; and 3) an offset, where applicable, of 1.4 cm. The beam is injected into full density air (with the scattering turned on and off to delineate stability properties), an on-axis channel, and an off-axis channel.

The Super-IBEX simulations assume a moderately tailored (2.5:1.0 over 7 ns), 5 MeV beam having: 1) a 35 ns temporal profile with a 15 ns linear

* Work supported by the Defense Advanced Research Projects Agency, ARPA Order No. 4395, Amendment No. 80, monitored by the Naval Surface Warfare Center.

** Address: Berkeley Research Associates, Springfield, VA 22150

rise, 5 ns plateau, and 15 ns fall; 2) a nominal radius of 1.5 cm; 3) a constant, low frequency (33 MHz) initial hose perturbation with a 2 mm amplitude; and 4) currents of 10, 20, 30, and 40 kA. The channel characteristics are: 1) a minimum density equal to $0.2\rho_o$; 2) a 4.0 cm radius; and 3) an offset, where applicable, of 1.5 cm. The beam was injected into full density air, reduced density ($0.2\rho_o$) air, an on-axis channel, and offset from the channel axis.

In both cases, tracking distances and hose e-folding distances are computed. The channel/beam offset is initiated in the y-direction so hose e-folding distances are obtained from the x-centroid motion. Sample results for the 20 ns slice of each beam (spanning the designated currents) are shown in the following table:

PULSERAD		
Propagation Medium	Tracking Distance (cm)	Hose e-folding Distance (cm)
Full air	---	29 - 34
Centered channel	---	23 - 27
Offset channel	28 - 33	18 - 27
Super-IBEX		
Propagation Medium	Tracking Distance (cm)	Hose e-folding Distance (cm)
Full air	---	40 - 96
0.2 atm air	---	40 - 80
Centered channel	---	$\geq$ 200
Offset beam	21 - 28	144 - 164

The simulation results follow the generally expected trends. For example, higher beam currents result in increased hose motion (shorter e-folding distances) as well as stronger tracking forces (shorter tracking distances).

The PULSERAD simulations show tracking distances comparable to hose e-folding distances. The centered-channel cases appeared to be somewhat more unstable than the full-density-air cases. Both results are consistent with

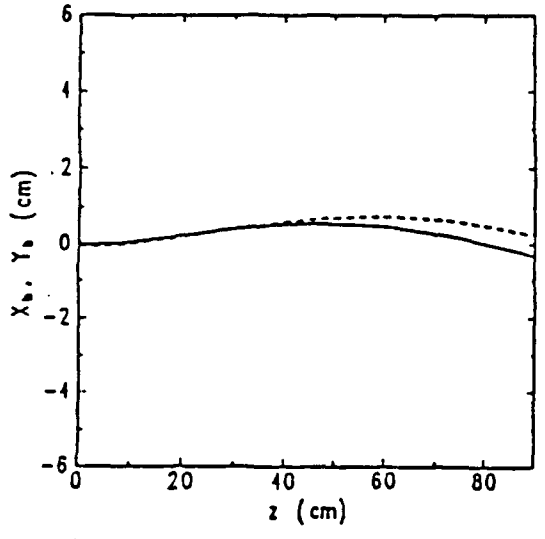

Fig.1. 7 kA PULSERAD beam injected into full density air; y-centroid (dashed line), x-centroid (solid line).

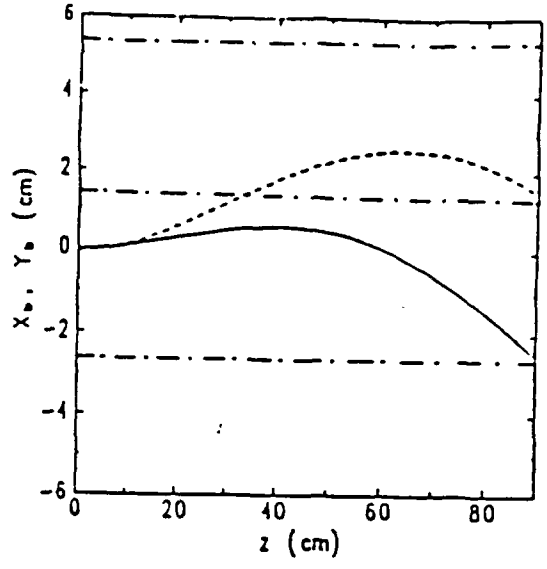

Fig.2. 7 ka PULSERAD beam injected into offset channel; same as in Fig. 1, channel edges and axis (dot-dashed line).

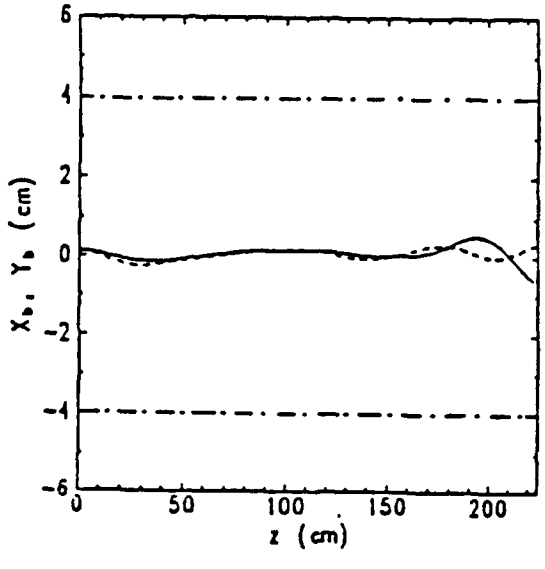

Fig.3. 30 kA Super-IBEX beam injected along channel axis; same as in Fig. 2.

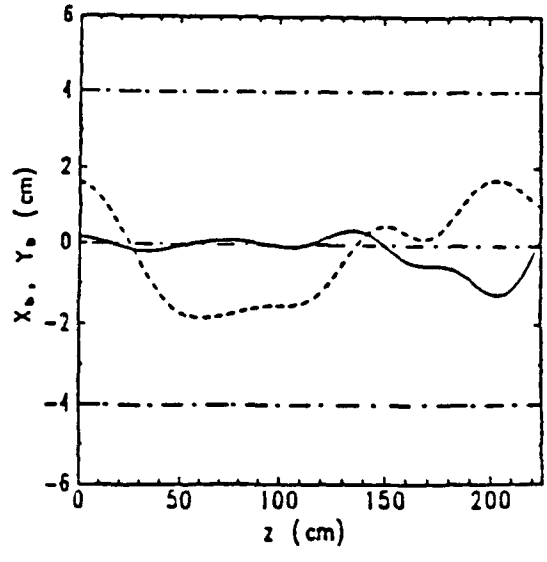

Fig.4. 30 kA Super-IBEX beam injected at an offset from channel; same as in Fig. 2.

those found in the experiment.[2] A comparison of Figs. 1 and 2 shows the effect of an offset channel on the beam. Not shown in the figures are cases for the beam in a centered channel and the beam in air with the scattering turned off. These latter cases have nearly identical current and radius profiles and similar hose instability amplitudes. Thus, the apparent increase in hose growth in the presence of the channel is primarily due to the reduction in scattering. When hose growth is properly scaled to the number of betatron wavelengths propagated by the beam, the channel has virtually no effect. Over 90 cm, the beam deflection for these cases is comparable to the x-deflection seen in Fig. 2 which, in turn, is greater than that shown in Fig. 1.

The Super-IBEX simulations show tracking distances much shorter than the characteristic hose distances. Figure 4 is a dramatic example of the effect of the tracking force. A beam injected off of the channel axis is drawn toward the channel, overshoots, rides the far edge, is drawn back into the channel, and begins to oscillate. A beam injected along the channel axis is stabilized over a substantial distance (225 cm); see Fig. 3. As seen in the table, the beam is much less unstable in the centered channel than in full density air even though it has traveled more betatron wavelengths. There are two reasons for this apparent stabilization. First, the higher currents in Super-IBEX result in much more return current flow at the edge of the channel which is a well-known stabilizing effect. In addition, the Super-IBEX runs assume a constant, low frequency perturbation, representative of that expected in the experiment.[3] These perturbations do not couple to the hose instability as well as the higher frequency modes used to initialize the PULSERAD simulations. These simulations are a clear demonstration of the importance of limiting high frequency perturbations in stability and tracking experiments.[1]

1. R. Hubbard, S. Slinker, and R. Taylor, "Sensitivity of Hose Instability to Frequency of Initial Perturbations in Low and High Current Beams", these proceedings.

2. D. Murphy, "Evidence of Hose Instability in Density Channels", these proceedings.

3. R. Meger, J. Antoniades, and T. Peyser, private communication.

SENSITIVITY OF HOSE INSTABILITY TO FREQUENCY OF INITIAL PERTURBATION IN LOW AND HIGH CURRENT BEAMS*

R. F. Hubbard, S. P. Slinker and R. D. Taylor**
Plasma Physics Division, Naval Research Laboratory, Washington, DC 20375

I. INTRODUCTION

Most studies of resistive hose instability in propagating electron beams have assumed that the frequency spectrum of the initial perturbation cannot be experimentally controlled. However, Fawley has pointed out that for the ATA Multi-Pulse Propagation Experiment (MPPE), the relative amplitudes of low frequency sweep and high frequency (BBU-induced) perturbations are sensitive to the guide field, B_z, in the accelerator. Increasing B_z reduces the growth of BBU but enhances corkscrew-induced sweep.

We have used the SARLAC hose instability code[1] to determine which class of perturbations is the more dangerous. SARLAC models beam propagation in the atmosphere using the doppler-shifted coordinates z and $\zeta = ct - z$. Here, z is the propagation distance in air and ζ is the distance from the beam head. A BBU-like 830 MHz perturbation, $X(\zeta,z=0)$, is imposed in the x-direction using an asymptotic BBU growth model from Caporaso.[2] A low frequency (LF) sweep perturbation is imposed in the y-direction. In general, the hose growth in the x-direction dominates even when its initial amplitude is substantially lower, suggesting that ATA should be operated with a high B_z. Similar results have been obtained by Feinstein and Keeley.[3] HF perturbations also generate more instability growth in RADLAC simulations. These HF perturbations initiate hose growth in the "neck" of the beam where the dipole decay length is relatively short. Since the local betatron wavelength is usually long in this region, an HF perturbation may generate <u>low</u> frequency oscillations in z.

II. ATA HOSE SIMULATIONS

<u>BBU perturbation model:</u> Following Caporaso,[2] the beam exits the accelerator with a displacement $X(\zeta,z=0) = X_0\exp(KNI_b(\zeta)Z_\perp\omega_0/B_z)\sin(\omega_0\zeta/c)$. Here, I_b is the beam current in kA, the cavity impedance $Z_\perp = 30\ \Omega$, $\omega_0/2\pi = 8.3\times10^8\ sec^{-1}$, the number of cavities $N = 50$, $B_z = 1$-3 kG, $X_0 = 10^{-4}$ cm and

the coefficient $K = 1.16 \times 10^{-13}$ kG-sec(kA-ohm)$^{-1}$. The beam is assumed to have an energy of 10 MeV with the current ramping to its nominal value $I_0 = 6$ or 8 kA over a distance $\zeta_r = 360$ cm. The injected radius and emittance profiles follow the form shown in Fig. 4 of Ref. 4 which are generated from a FRIEZR simulation of a 5 mtorr passive IFR conditioning cell.

Corkscrew or sweep perturbation model: Low frequency sweep or corkscrew arises from the coupling between energy variations $\Delta\gamma$ within the pulse and field or alignment errors. This produces a phase advance, $\delta\phi = (\Delta\gamma/\gamma)\int k_c dz$, where the cyclotron wavenumber k_c is proportional to B_z. For $\delta\phi << 1$, the phase advance and sweep amplitudes are proportional to B_z. In SARLAC, this effect is modeled by imposing an initial perturbation in the y-direction given by $Y(\zeta, z=0) = \alpha B_z \zeta$. The coefficient α is chosen to be 3×10^{-5} (kG)$^{-1}$.

Results: Four long SARLAC simulations were run with the parameters described above. Cases A1, A2 and A4 were for $I_0 = 6$ kA and $B_z = 1$, 1.5 and 3 kG, respectively, while Case A3 used an 8 kA beam with a 1.5 kG guide field. Results are summarized in the table below. The displacements X and Y are taken in the beam tail at $\zeta = 750$ cm (25 nsec) and are tabulated at injection ($z = 0$) and at $z = 5.4$ m.

Case	I_o	B_z	X(0)	Y(0)	X(5.4m)	Y(5.4m)
A1	6 kA	1.0 kG	0.010 cm	0.022 cm	0.31 cm	0.12 cm
A2	6	1.5	0.0035	0.034	0.20	0.12
A3	8	1.5	0.010	0.034	0.67	0.14
A4	6	3.0	0.0006	0.068	0.11	0.12

Figure 1 plots the initial perturbations $X(\zeta,0)$ and $Y(\zeta,0)$ for Case A2, showing that the HF perturbation (solid curve) is an order of magnitude lower than the sweep perturbation (dashed curve). However, Fig. 2 shows that at $z = 6$ m, the HF modes induced in the x-direction have surpassed those in the y-direction. Increasing I_0 to 8 kA results in a substantial increase in X, both because the BBU-induced initial perturbation is larger and because the higher current beam travels more betatron wavelengths. The resulting hose amplitudes are shown in Fig. 3. The results suggest that ATA should be operated with a relatively high guide field to suppress BBU and that relatively large sweep amplitudes may be tolerated without initiating serious instability growth.

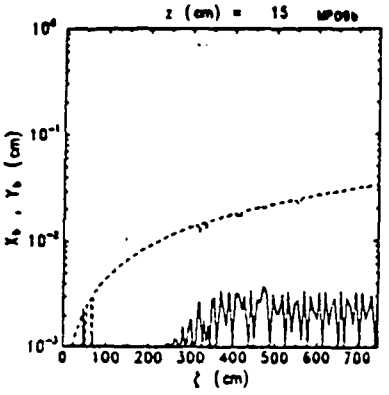

Fig 1. Initial displacement $X(\zeta,0)$ and $Y(\zeta,0)$ (solid and dashed lines): Case A2

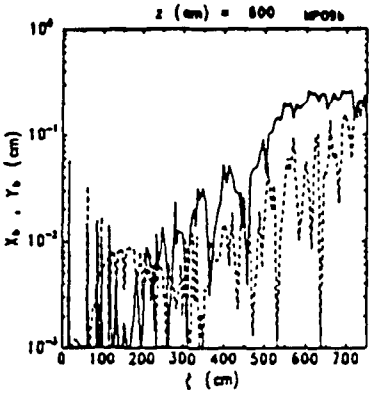

Fig 2. $X(\zeta)$ and $Y(\zeta)$ at z = 6m for Case A2. BBU-induced hose is stronger (solid line).

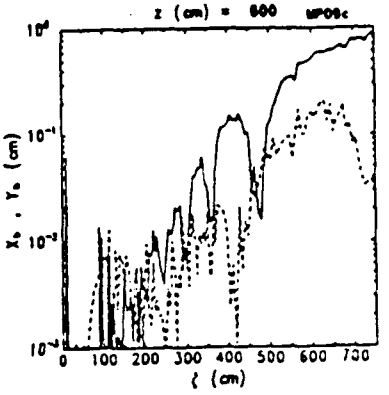

Fig 3. $X(\zeta)$ and $Y(\zeta)$ at z = 8m or Case A3. I_0 is raised to 8 kA; beam is more unstable.

III. RADLAC HOSE INSTABILITY SIMULATIONS

Overview: Both HF and LF perturbations are produced in RADLAC even though BBU is thought to be unimportant. A series of SARLAC simulations were performed using a 0.02 cm, 830 MHz HF perturbation in x and a 0.2 cm (at ζ = 900 cm) sweep perturbation in y. Nominal beam parameters in the simulations were I_0 = 25 kA, γ_0 = 41 (ramped in some cases), beam radius a_b = 2 cm, rise length ζ_r = 300 cm and normalized emittance taper ε_t = 2-4.

RADLAC simulation results: Six simulations were performed as described in the table below. E_{min} and E_{max} define the range of the energy ramp, and X_{max} and Y_{max} are the maximum hose amplitudes at ζ = 900 cm and $z < 12$ m.

Case	E_{min}	E_{max}	η_t	Comment	X_{max}	Y_{max}
R1	20 MeV	20 MeV	4	-	0.5 cm	0.5 cm
R2	20	20	4	a_b=1.5cm	2.5	0.8
R3	5	20	2	-	> 20	> 5
R4	5	20	4	-	4.5	1.5
R5	5	20	4	Y_0=0.02cm	4.5	0.6
R6	10	20	4	Faster γ-ramp	1.1	0.4

As in the ATA simulations, the high frequency modes dominate even though they are initiated at a smaller amplitude. Comparing Cases R1 and R3, it is apparent that relying on the natural tailoring which comes about from the energy ramp may lead to unacceptably large hose amplitudes. This is, in part,

because the head is so hot that it is quickly lost, leaving behind a poorly-tailored beam. Even when the 4:1 emittance variation is restored to a beam with a γ-ramp (Case R4), the beam is more unstable than in the constant energy case. Figure 4 plots X(z) and Y(z) at ζ = 675 cm for Case R4, showing an initial damping of the LF mode followed by an eventual coupling to the faster-growing HF mode. Hose amplitudes versus ζ at z = 120 cm are shown for this case (Fig. 5) and for the more unstable weakly-tapered Case R3 (Fig. 6).

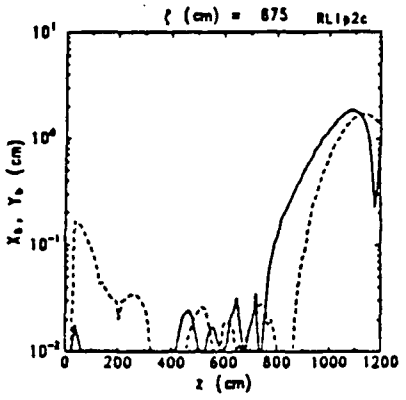

Fig 4 X(z) and Y(z) at ζ = 675cm for RADLAC Case R4. Note initial decay in Y (dash line).

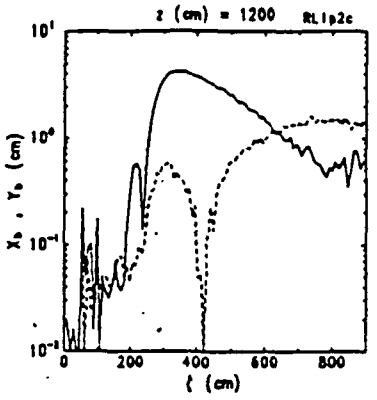

Fig 5. X(ζ) and Y(ζ) at z = 12 m for Case R4. HF mode (solid line) dominates.

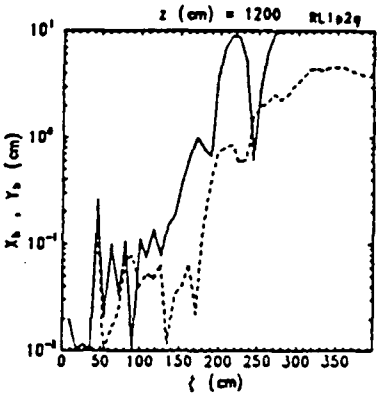

Fig. 6. X(ζ) and Y(ζ) at z = 12 m for Case R4 (weaker taper). Note shorter pulse length.

IV. CONCLUSIONS AND REFERENCES

For both ATA and RADLAC, high frequency perturbations appear to couple more strongly to the resistive hose instability and should be suppressed if possible even at the expense of higher sweep amplitudes.

1. G. Joyce, R. Hubbard, M. Lampe and S. Slinker, J. Comp. Phys. 81, 193 (1989).
2. G. Caporaso, A. Cole and K. Struve, LLNL Report UCID-88262 (1983).
3. D. Keeley, "Hole Boring and Hose Instability Studies for ATA MULti-Pulse Experiment," these proceedings.
4. R. Hubbard et al, "Beam Conditioning Options for the ATA Multi-Pulse Expeiment," these proceedings.

*Supported by the Defense Advanced research Projects Agency, ARPA Order No. 4395, Amendment 80, Monitored by the Naval Surface Warfare Center,

**Berkeley Research Associates, Springfield, VA 22150

PULSE DECOUPLING USING ATA*

R. Fernsler, S. Slinker, and R. Hubbard
Beam Physics Branch, Plasma Physics Division
Naval Research Laboratory, Washington, D.C.

INTRODUCTION

As the lead pulse propagates, its energy and geomagnetic gyroradius decrease while its radius increases. The density channel formed by the pulse thus becomes progressively curved but broader and more shallow. As a consequence, a follower beam pulse is predicted[1] to decouple from the lead-pulse channel as the channel tracking force becomes weak (in the beam head) relative to the geomagnetic force. The follower pulse then becomes the new lead pulse and constructs its own channel. Although predictable pulse decoupling is a critical applications issue, it has received only cursory analytic attention and no experimental or numerical verification.

In this paper we consider using ATA for studying pulse decoupling. A series of four, closely spaced beam pulses would be used to create a density channel in atmospheric air. Prior to the fifth pulse, a fixed external magnetic field ~ 1 Gauss would be applied. Because the density channel weakens with range z, the tracking force would weaken until the fifth pulse ultimately left the channel created by its predecessors.

ISSUES

Pulse decoupling is a complicated process involving channel evolution and the mutual interaction of three forces: an external (geomagnetic/centrifugal) deflection force generated by the geomagnetic field, channel curvature, and pulse-to pulse energy differences; a channel tracking force[2] arising from beam-generated ionization, air chemistry, and the depression in channel gas density; and a body coupling force that causes the beam body to follow the head (and also drives the resistive hose instability). Existing codes should be capable of modeling all of these forces with only minor modifications. Experimental verification, however, is more difficult.

An ideal pulse-decoupling experiment should address several key issues: (1) How strong can the external force be before channel tracking and pulse

*Work supported by the Defense Advanced Research Projects Agency, ARPA Order No. 4395, Amendment 80, monitored by the Naval Surface Warfare Center

coupling are destroyed? (2) What are the effects of beam tilt on the hose instability and hole-boring? (3) How much emittance tailoring, for hose suppression, can be tolerated? (4) Is pulse decoupling a smooth and predictable process, and when and where does it occur? And (5), to what extent does an external force enhance nose erosion? Answering any of these questions requires a beam that remains stable and tightly pinched as it comes to equilibrium with the various deflection forces.

SIMULATION

To assess the potential of ATA for studying pulse decoupling, we used the SARLAC code to simulate a single ATA pulse propagating into a preexisting channel. The beam parameters at injection were: peak current 6 kA; half-current radius $R_{1/2}$ = 0.5 cm in the beam body; emittance tailoring of 4-to-1 over 325 cm; matching current I_m = 3 kA; and displacement x = 0.75 cm from the channel axis. The density channel was Gaussian with a radius of 1.5 cm and on-axis density of 0.2 atm. The channel was uniform in z and centered within a conducting pipe of radius b = 32 cm. A fixed deflection force of 3 Gauss was applied. The choice of a large pipe radius and large deflection force is explained below.

RESULTS

Figure 1 shows the beam centroid (x,y) as a function of distance behind the beam head, ζ = ct-z, at several propagation distances z in the absence of a channel. The beam tilts in response to the wall forces which become strong in the body and retard its off-axis motion. The body consequently remains closer to the pipe axis than does the head. [The apparently modest drift of beam slices at $\zeta < 50$ cm is an artifact of beam expansion and scrape-off.] A significant reduction in the pipe radius or deflection force is undesirable because the wall forces would then obscure the deflection force. Increasing the pipe radius to $b > 1$ m would virtually eliminate the wall forces.

Figure 2 plots the beam centroid (x,y) with the channel present, and illustrates the effect of the channel tracking force. This force, together with the wall force, exceeds the external force of 3 Gauss at $\zeta \gtrsim 120$ cm, and pulls the beam body into the channel. The beam head, however, is pulled out of the channel by the external deflection force. Observe that the beam tilt is increasing at z = 3 m, indicating that the beam has not yet reached

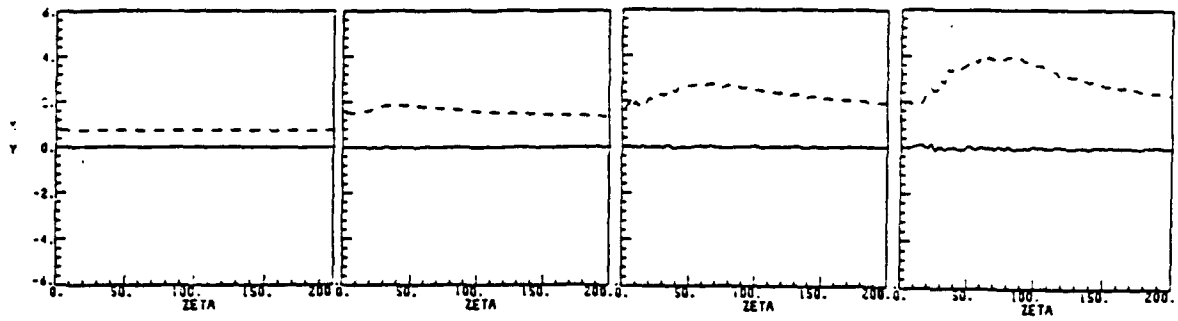

Fig. 1. Beam centroid (x,y) at z = 0, 1.5, 2.25, 3 m without a channel.

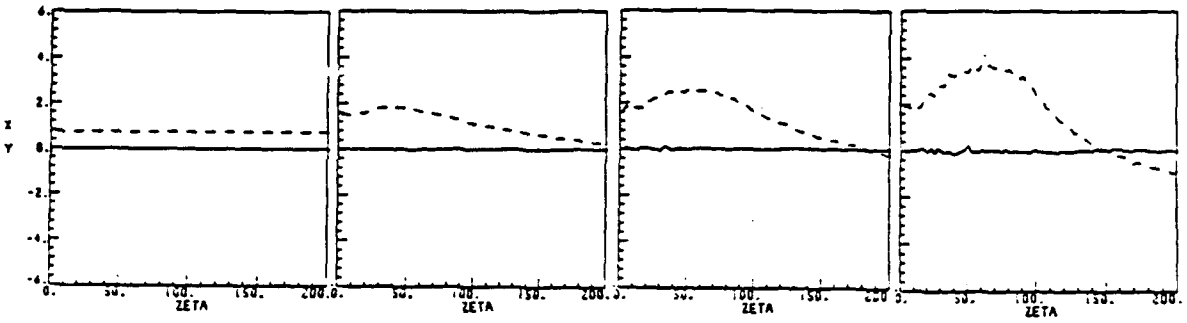

Fig. 2. Beam centroid (x,y) at z = 0, 1.5, 2.25, 3 m with a channel.

equilibrium. Moreover, whether the beam body remains in the channel or follows the ejected head is unclear. Hence, this simulation demonstrated channel tracking but not pulse decoupling. Range extension is evident in Fig. 3 in that the beam expands less when propagating in the channel.

CONCLUSION

Simulation of a simple pulse-decoupling experiment for ATA revealed several difficulties, the principal ones being the wall forces and the need for the beam to propagate a long distance before pulse decoupling can be observed. A potential solution to the latter problem is to inject the beam on axis in the channel and turn on the external deflecting force gradually in z.[3] The beam should then remain in near equilibrium with the external, tracking, and coupling forces.

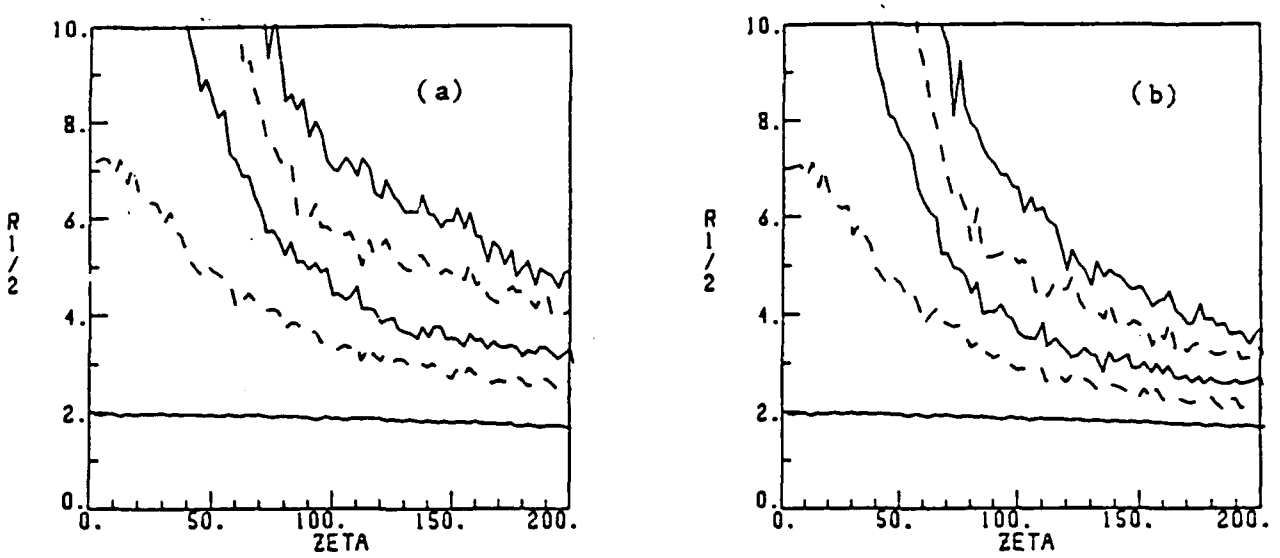

Fig. 3. $R_{1/2}$ without (a) and with (b) a density channel. Plots at z = 0, 0.75, 1.5, 2.25, and 3 m.

REFERENCES

1. R.F. Fernsler, "Pulse Decoupling from WIPS Channels," Proceed. of Annual DARPA Review, Monterey, California, Sept. 28 - Oct. 2, 1987.
2. R.F. Fernsler, "Tracking of Electron Beams in Low-Density Channels (U)", NRL Memorandum Report 6041 (Confidential), 1987.
3. M. Lampe, private communication.

Electron Energy Deposition in O^+.*

R.D. Taylor,** A.W. Ali, and S.P. Slinker
Beam Physics Branch, Plasma Physics Division
Naval Research Laboratory, Washington, D.C. 20375

A discrete, time-dependent energy deposition model is used to study high-energy electron-beam (100 eV to 10 MeV) deposition in O^+. Details of the deposition code and applications to other gases have been reported previously[1-6] and published elsewhere.[7-9] Secondary electron distributions are obtained by solving a time-dependent, relativistic Boltzmann equation. These distributions relax to steady-state results from which yield spectra, production efficiencies of specific states, energy partitioning, and mean energies per electron-ion pair production (W) are computed. Loss functions are calculated and compared to Bethe's relativistic equation.[10] The model predicts W is approximately 72 eV for O^+ over a wide range of beam energies and background ionization fractions. The effects of inner shell ionization and excitation have been included in the deposition model. These effects result in an increase in W of approximately 17% for energies above 10 keV. While the present study has focused on beam sources, W is observed to change for energies below 1 keV if the source electrons are assumed to be completely stopped by the medium.

The Boltzmann equation describes a spatially homogeneous electron beam impinging upon a single component gas. Electric and magnetic field effects due to the beam are neglected. The effects of inelastic and ionizing collisions are accounted for, however, elastic and superelastic collisions between the electrons and background gas are neglected. The gas density and source term are time independent. Energy loss to the plasma electrons is included by means of a loss funtion. Coupling to the radiation field is neglected.

For deposition in O^+, energy loss to the $2p^3\ ^2D^o$ and $2p^3\ ^2P^o$ states, all $n = 3$ states, 2 effective Rydberg series ($n \geq 4$) states, and the $^3P\ O^{++}$ state is considered. Analytic forms for the relevant excitation and ionization cross sections have been obtained. A detailed discussion of these forms, their reduction to well-known theoretical results, and their relative accuracy in

* Work supported by the Defense Advanced Research Projects Agency, ARPA Order No. 4395, Amendment No. 80, monitored by the Naval Surface Warfare Center.

** Address: Berkeley Research Associates, Springfield, VA 22150

comparison to existing measurements and calculations is given elsewhere.[9,11] The K-shell ionization threshold is 565 eV and it is assumed that all Auger electrons are produced at 475 eV.

Results are generated for a beam flux of 1.99×10^{18} cm^{-2} sec^{-1}, a background density of 2.46×10^{19} cm^{-3}, and various fractional ionizations (zero unless otherwise noted). Figure 1 shows the loss function, L(T), (neglecting inner-shell effects) and its components for energies up to 10 MeV for O^+. Most of the energy goes into producing secondary electrons, while loss to excitation is significant only below the ionization threshold. Also shown is a comparison with Bethe's relativistic loss function, $L_B(T)$. For energies greater than 1 keV, L(T) and $L_B(T)$ are in close agreement. In principle, energy loss of an electron traversing a material is lessened because of polarization of the medium. This density effect is small for the energies in the present studies. The inclusion of inner-shell effects and the resultant changes to the loss function are shown in Fig. 2. For example, for energies greater than 1 keV, the inner shell contribution exceeds loss to excitation.

Average excitation, ionization, and secondary energies are presented in Fig. 3. There is very little change in $\bar{I}$ and $\bar{E}_e$ for energies greater than ~ 100 eV. Asymptotically, $\bar{I}$ = 35.1 eV and $\bar{E}_e$ = 20.6 eV for O^+. K-shell ionization increases $\bar{I}$, also shown in Fig. 3.

The steady-state values of W (with and without inner-shell ionization) for beam energies, T_b, ranging from 100 eV to 10 MeV are shown in the following table:

T_b (eV)	10^2	10^3	10^4	10^5	10^6	10^7
W(eV): L	80.5	72.3	72.3	72.2	71.3	70.0
W(eV): L & K	----	74.2	82.0	84.2	84.9	84.9

These values are nearly constant over an large energy range. The near constancy of W at energies $\geq$ 1 keV is well-known. The increase in W which accompanies the addition of K-shell ionization is a direct conequence of the increased $\bar{I}$. Figure 4 shows a comparison between W for beam electrons and

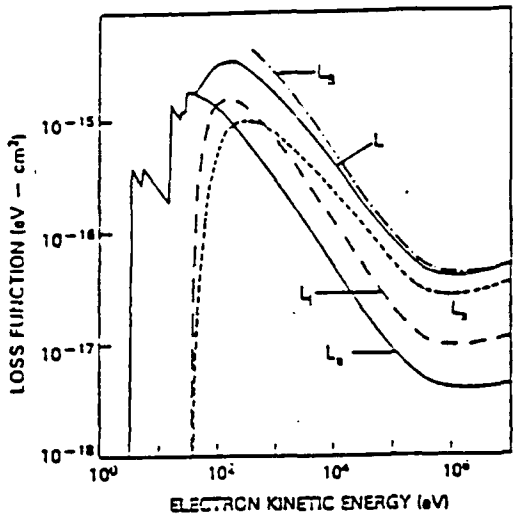

Fig.1. Excitation, L_e, ionization, L_i, and secondary contributions, L_s, to the total loss function, L, versus Bethe's formula, L_B.

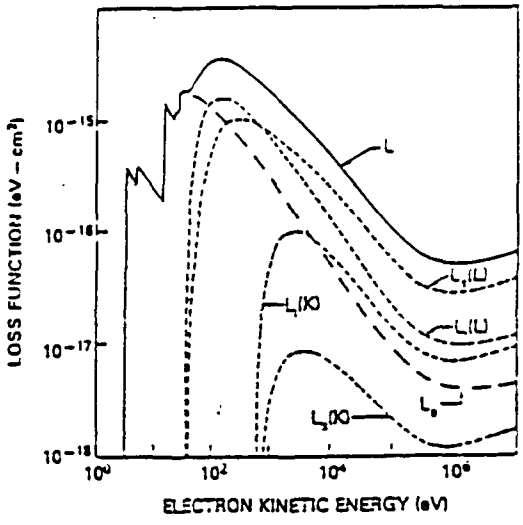

Fig.2. L- and K-shell contributions to the loss function.

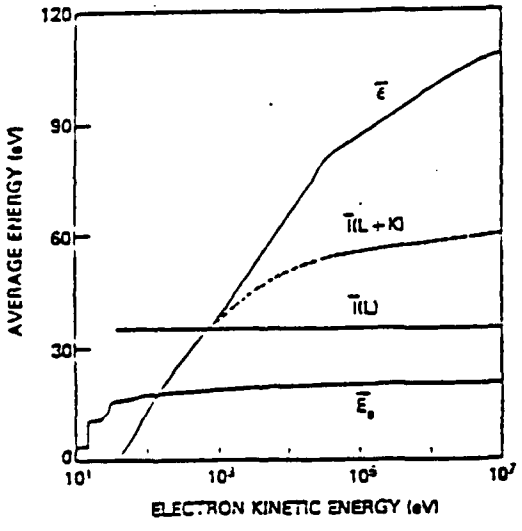

Fig.3. Average excitation, $\bar{E}_e$, ionization, $\bar{I}$, and secondary energies, $\bar{\varepsilon}$.

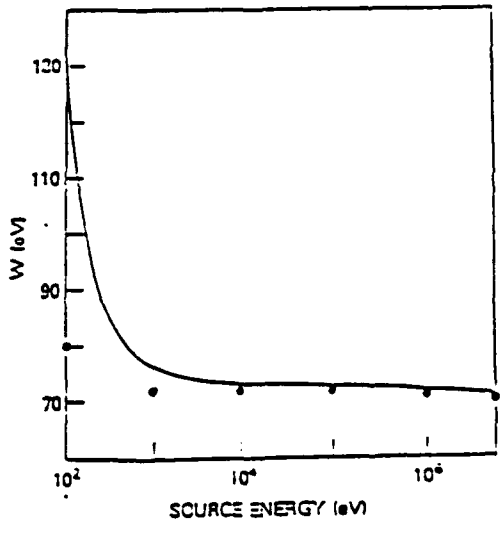

Fig.4. W for beam (solid line) and stopped (dots) electrons.

for completely-stopped electrons. There is very little difference for energies greater than 10 keV, but significant differences below.

Other results obtained from the present analysis and discussed in detail elsewhere[9] include the following:

Relaxation of the distribution function to a steady-state is non-uniform, i.e. energy-dependent. Intermediate energies (~ 100 eV) relax first, followed by the lower part of the spectrum (~ 10 eV, but greater than the lowest excitation energy), and, finally, the high energies ($\geq$ 1 keV).

Production efficiencies (per electron-ion pair created) for excited states are nearly constant for the beam energies considered.

The results show some sensitivity to background ionization fraction. In particular, the distribution function is insensitive to changes in the background for energies greater than ~ 20 eV, but highly sensitive for lower energies. Energy lost to background electrons increases with increasing numbers of these electrons, however, W remains nearly constant until the fraction approaches 10^{-2}.

Finally, we note that the results of this study are sensitive to the magnitude of the K-shell cross section, when included. Unfortunately, no experimental data on K-shell cross sections or W (for O^+) exists so the choice is not unique.

1. S. Slinker and A.W. Ali, Proceedings of the SDIO/DARPA Annual Propagation Review, Alburquerque, New Mexico (1986).
2. S. Slinker and A.W. Ali, "Electron Energy Deposition in Atomic Oxygen", NRL Memorandum Report 5909, Washington, D.C. (1986).
3. R.D. Taylor, S.P. Slinker, and A.W. Ali, "Electron Energy Deposition in Atomic Nitrogen", NRL Memorandum Report 6087, Washington, D.C. (1987).
4. R.D. Taylor, S. Slinker, and A.W. Ali, Proceedings of the SDIO/DARPA/Services Annual Propagation Review, Monterey, California (1987).
5. S. Slinker, R. Taylor, and A.W. Ali, Bull. Am. Phys. Soc. 32, 1947 (1987).
6. A.W. Ali, S. Slinker and R.D. Taylor, BEAMS '88 Seventh International Conference on High-Power Particle Beams, Karlsruhe, Germany (1988).
7. S.P. Slinker, R.D. Taylor, and A.W. Ali, J. Appl. Phys. 63, 1 (1988).
8. R.D. Taylor, S.P. Slinker, and A.W. Ali, J. Appl. Phys. 64, 982 (1988).
9. R.D. Taylor, A.W. Ali, and S.P. Slinker, "Energy Deposition in O^+ by High-Energy Electron Beams", J. Appl. Phys. (in press).
10. H.A. Bethe, Handbuch der Physik, Vol. 24, p. 273, Springer, Berlin (1933).
11. R.D. Taylor and A.W. Ali, "Excitation and Ionization Cross Sections for Electron-Beam Energy Deposition in High Temperature Air", NRL Memorandum Report 6013, Washington, D.C. (1987).

Transverse Two Stream Instability*

Glenn Joyce and Martin Lampe

Beam Physics Branch, Plasma Physics Division
Naval Research Laboratory, Washington, D.C.

INTRODUCTION:

A relativistic electron beam propagating through a diffuse plasma can interact strongly with the plasma resulting in a change of the properties of the beam. The beam can generate electrostatic wakefields in the plasma causing the plasma to act as a transformer and move energy from one region of the beam to another. This aspect of the wakefield effect is primarily axisymmetric and has been treated extensively in the past. Another aspect is the interaction of nonaxisymmetric perturbation of the plasma with the beam. The result of this type of perturbation is an m = 1 instability. For a beam propagating in a diffuse plasma of constant density, the instability is absolute in the beam frame and has a large growth rate. However, if the beam is propagating in an IFR channel, the instability is convective and under most circumstances the perturbations will pass through the beam before the disturbances have grown large enough to disrupt the beam. The reason for the change from absolute to convective is that for a channel of varying density, the beam electrons oscillate with different frequencies depending on their radial positions giving rise to phase-mix damping. We have studied the transverse instability both analytically and numerically using the ELBA three-dimensional particle simulation code.

DISPERSION RELATION:

We begin with the linearized cold fluid equations in the electrostatic-magnetostatic approximation and consider m = 1 perturbations.

$$\frac{\partial n_1}{\partial t} + \vec{v}_1 \cdot \nabla n_o + n_o \nabla \cdot \vec{v}_1 = 0,$$

$$\frac{\partial \vec{v}_1}{\partial t} = \frac{q}{m} \vec{E} - \nu \vec{v}_1,$$

$$E_r = - \frac{\partial \phi}{\partial r}, \quad E_\theta = - \frac{i\phi}{r},$$

and

$$\nabla_\perp^2 \phi = -4\pi q \, (n + n_b).$$

We skip the details of the derivation and write the result. If we consider perturbations of the type $ei(\omega\zeta + \Omega z)$, the dispersion relation becomes

$$\frac{\omega(\omega - i\nu)}{\omega_p^2} = 1 - \frac{1}{4}\left(\frac{a_b}{a_n}\right)^2 \frac{\omega_b^2}{\gamma c^2}\left\langle \frac{1}{\Omega_\beta^2 - \Omega^2}\right\rangle,$$

where $\omega_p^2 = \dfrac{4\pi n_o e^2}{m_e}$, $\omega_b^2 = \dfrac{4\pi n_b e^2}{m_e}$,

$\Omega_\beta^2 = \dfrac{1}{2}\dfrac{\omega_{ch}^2}{\gamma c^2}$, $\omega_{ch}^2 = \dfrac{4\pi n_{ch} e^2}{m_e}$,

$\left\langle \dfrac{1}{\Omega_\beta^2 - \Omega^2}\right\rangle$ = average over betatron frequency.

For the case in which there is no channel $\omega_{ch}^2 = \omega_p^2$, so all beam electrons have the same betatron wavelength. Using $a_b^2 n_b = a_n^2 n_o$, the dispersion relation becomes ($\nu \to 0$),

$$\frac{\omega^2}{\omega_p^2} = 1 - \frac{1}{2}\frac{1}{1 - \Omega^2/\Omega_\beta^2},$$

which is the result of Yu and Sharp (private communication).

For the case of a beam in an IFR channel and a diffuse plasma, the channel density varies with r leading to a spread in betatron wavelength. Also $n_{ch} >> n_o$, so

$$a_b^2 n_b = a_n^2 n_o + a_{ch}^2 n_{ch} = a_n^2 n_o/(1-f_{ch}).$$

We write $\Omega^2 = \Omega/\Omega_{\beta o}$ and $\eta = \Omega_\beta/\Omega_{\beta o}$. Then

$$\frac{\omega}{\omega_p} = \pm\left[1 - \frac{1}{2}\left(\frac{n_o}{n_{ch}}\right)\frac{1}{1-f_{ch}}\left\langle\frac{1}{\eta - \tilde{\Omega}^2}\right\rangle\right]^{1/2}$$

$$\approx \pm 1 \pm \frac{1}{4}\left(\frac{n_o}{n_{ch}}\right)^2 \frac{1}{1-f_{ch}}\left\langle\frac{1}{\eta - \tilde{\Omega}^2}\right\rangle$$

which makes the dispersion relation look like a hose dispersion relation.

If we take the spread mass model for a Bennett-like channel, we can estimate the effect of the instability as $\omega_i/\omega_o = (n_o/n_{ch})\ 3\pi/8$. Writing the beam length $\zeta_{max} = N\ 2\pi c/\omega_o$, where N is the number of plasma wavelengths in the beam, we find

$$\text{Amplitude} = e^{(n_o/n_{ch})/(1-f)3\pi^2/4\ N}.$$

For Delphi N = 28 and $n_o/n_{ch} = 10^{-3}$ so we expect the amplitude growth to be less than the beam radius.

PARTICLE SIMULATION:

We have simulated the instability with the ELBA code considering beam propagating in diffuse plasmas with and without IFR channels. For these runs, the simulation parameters were I = 1 kA, $\gamma = 4$, and $a_b = 1$ cm. The simulations were for either a constant density background plasma or a channel with $a_{ch} = 1$ cm, and $f_{ch} = .5$ and a constant density background plasma. The beam and plasma densities are chosen such that $\lambda_\beta = 104$ cm and $\lambda p_1 = 37$ cm.

The simulation results for the constant density case are shown in Figs. 1-4. For a constant background plasma after some propagation distance, a purely growing mode appears. Figure 1 is a plot of the centroid displacement as a function of z for constant ζ. From this we have measured a frequency of $\tilde{\Omega} = .91$. The growth rate can be determined from Fig. 2 which is a plot of centroid displacement as a function of ζ for constant z. The growth rate determined from this plot is $\tilde{\omega}_i = 1.6$. According to the dispersion relation, if $\tilde{\Omega} = .91$, $\tilde{\omega}_i = 1.4$.

For the Bennett channel, the growth is much less violent and appears to stop before the beam oscillations become as large as the channel. Figure 3 is similar to Fig. 2, and Fig. 4 is similar to Fig. 2 except in this simulation, a channel of strength .5 was included. The effect of the channel is clearly to limit the growth of the instability.

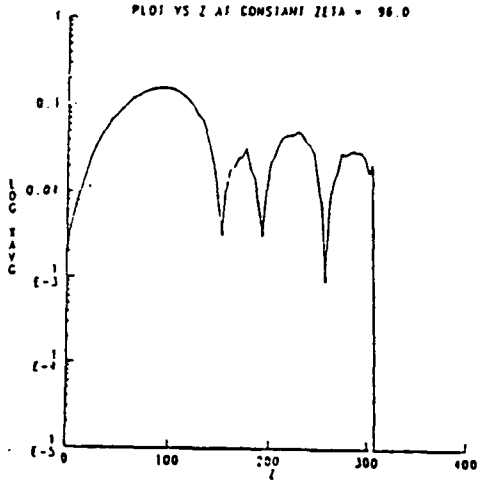

Figure 1

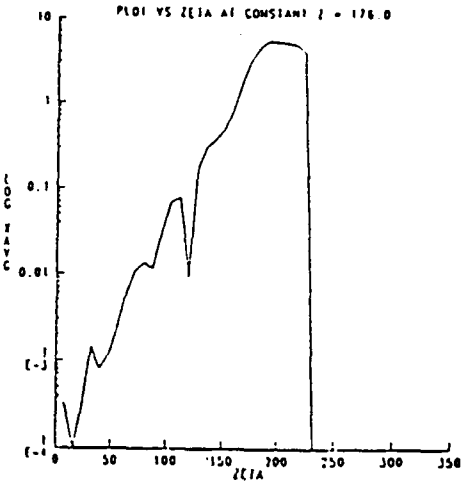

Figure 2

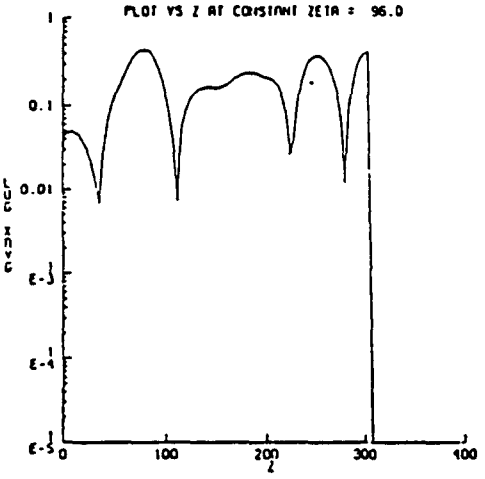

Figure 3

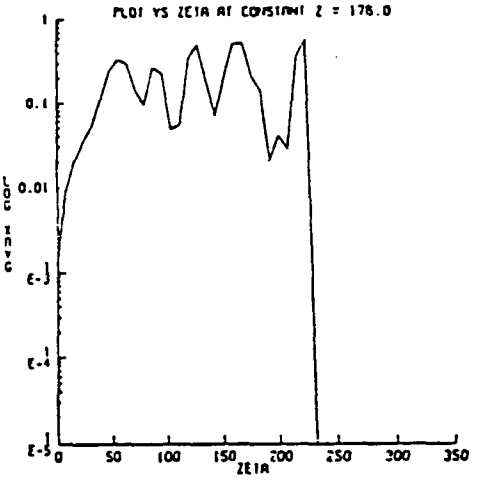

Figure 4

CONCLUSIONS:

A relativistic beam propagating through a diffuse plasma is unstable to transverse perturbations. For a plasma of constant density, the instability is quite severe and can rapidly disrupt the beam. The inclusion of an IFR channel with varying density can change the nature of the instability and cause the instability growth to stop before while the beam is still in the channel. We have presented and analytic theory and supporting simulations of this effect.

*Work supported by the Defense Advanced Research Projects Agency, ARPA Order No. 4395, Amendment 80, monitored by Naval Surface Warfare Center.

Distribution List*

Naval Research Laboratory
4555 Overlook Avenue, S.W.
Attn: CAPT J. J. Donegan, Jr. - Code 1000
Dr. M. Lampe - Code 4792 (20 copies)
Dr. T. Coffey - Code 1001
Head, Office of Management & Admin - Code 1005
Deputy Head, Office of Management & Admin - Code 1005.1
Directives Staff, Office of Management & Admin - Code 1005.6
Director of Technical Services - Code 2000
ONR - Code 0124
NRL Historian - Code 2604
Dr. W. Ellis - Code 4000
Dr. J. Boris - Code 4040
Dr. M. Picone - Code 4040
Dr. E. Oran - Code 4040
Dr. M. Rosen - Code 4650
Dr. M. Haftel - Code 4665
Dr. S. Ossakow - Code 4700 (26 copies)
Dr. V. Patel - Code 4701
Dr. A. Robson - Code 4708
Dr. M. Friedman - Code 4732
Dr. R. Meger - Code 4750
Dr. J. Antoniades - Code 4751
Dr. T. Peyser - Code 4751
Dr. D. Murphy - Code 4751
Dr. R. Pechacek - Code 4750.1
Dr. G. Cooperstein - Code 4770
Dr. A. Ali - Code 4780
Dr. D. Colombant - Code 4790
Dr. R. Fernsler - Code 4790 (20 copies)
Dr. I. Haber - Code 4790
Dr. R. F. Hubbard - Code 4790 (20 copies)
Dr. G. Joyce - Code 4790 (20 copies)
Dr. Y. Lau - Code 4790
Dr. S. P. Slinker - Code 4790 (20 copies)
Dr. P. Sprangle - Code 4790
Dr. C. M. Tang - 4790
Dr. J. Krall - Code 4790
B. Pitcher - Code 4790A
Code 4790 (20 copies)
Dr. S. Gold - Code 4793
Dr. C. Kapetanakos - Code 4795
Mr. P. Boris - SAIC (Code 5166)
Library - Code 2628 (22 copies)
D. Wilbanks - Code 2634
Code 1220

Advanced Scientific Concepts, Inc.
2441 Foothill Lane
Santa Barbara, CA 93105
Attn: Dr. Roger Stettner

Advanced Technologies Research
14900 Sweitzer Lane
Laurel, MD 20707
Attn: Mr. Daniel Weldman

The Aerospace Corporation
Mail Stop M2-269
P. O. Box 92957
Los Angeles, CA 90009
Attn: Dr. David L. McKenzie
Dr. Carl J. Rice

AFATL/DLJW
Elgin Force Base, FL 32542
Attn: MAJ Louis W. Seller, Jr.

Air Force Office of Scientific Research
Physical and Geophysical Sciences
Bolling Air Force Base
Washington, DC 20332
Attn: Major Bruce Smith

Air Force Weapons Laboratory
Kirtland Air Force Base
Albuquerque, NM 87117-6008
Attn: Dr. William L. Baker (AFWL/NTYP)
Dr. Brendan B. Godfrey
Dr. Inara Kuck

Applied Physics Laboratory
The Johns Hopkins University
Asst. to Dir. for Tech. Assessment
Johns Hopkins Road
Laurel, MD 20707
Attn: Dr. Samuel Koslov

Armed Forces Radiobiology
Research Institute
Chief, MRAD
NMC-NCR
Bethesda, MD 20814-5145
Attn: LCDR J. P. Jacobus

U. S. Army Ballistics Research Laboratory
Aberdeen Proving Ground, Maryland 21005
Attn: Dr. Donald Eccleshall (DRXBR-BM)
Dr. Anand Prakash
Dr. Clinton Hollandsworth

Avco Everett Research Laboratory
2385 Revere Beach Pkwy
Everett, Massachusetts 02149
Attn: Dr. R. Patrick
Dr. Dennis Reilly

Ballena Systems Corporation
P. O. Box 752
Alameda, CA 94501
Attn: Dr. Adrian C. Smith
Dr. William E. Wright

Ballistic Missile Def. Ad. Tech. Ctr.
P.O. Box 1500
Huntsville, Alabama 35807
Attn: Dr. H. Hawie (BMDSATC-1)
Dr. M. J. Lavan (BMDATC-E)
Mr. Dan Whitener

The Boeing Aerospace Company
MS-2E30
Box 3999
Seattle, WA 98124
Attn: Dr. Robert C. Milnor

Booz, Allen, and Hamilton
Crystal Square 2, Suite 1100
1725 Jefferson Davis Highway
Arlington, VA 22202-4136
Attn: Dr. Charles M. Huddleston

Brobeck and Associates
1235 10th Street
Berkeley, CA 94710
Attn: Dr. Francis C. Younger

Chief of Naval Material
Office of Naval Technology
MAT-0712, Room 503
800 North Quincy Street
Arlington, VA 22217
Attn: Dr. Eli Zimet

Commander
Space and Naval Warfare Systems Comman
National Center 1, Room 8E08
Washington, DC 20363-5100
Attn: RADM Robert L. Topping

Cornell University
369 Upson Hall
Ithaca, NY 14853
Attn: Prof. David Hammer

Defense Advanced Research Projects Agency
1400 Wilson Blvd.
Arlington, VA 22209
Attn: Dr. H. L. Buchanan
Dr. B. Hui

Defense Nuclear Agency
Washington, DC 20305
Attn: Dr. Muhammad Owais (RAAE)
Dr. Michael Frankle
Dr. R. Gullickson

Department of Commerce
National Inst.of Standards and Tech.
Building 245, B-102
Washington, DC 20234
Attn: Dr. Mark A. D. Wilson
Dr. Steven M. Seltzer

Department of Energy
Washington, DC 20545
Attn: Dr. Wilmot Hess (ER20:GTN,
High Energy and Nuclear Physics)
Mr. Gerald J. Peters (G-256)

Department of the Navy
Chief of Naval Operations
The Pentagon
Washington,DC 20350
Attn: CAPT T. L. Sanders (OP981N3)
LCDR John Stanovich (OP981SDI)
LCDR Donald Melick (OP981SD)
Dr. Steve Bravy (OP981SDI)
Mr. Greg Montieth

Directed Technologies, Inc.
4001 Fairfax Drive, Suite 775
Arlington, VA 22203
Attn: Mr. Ira F. Kuhn
Dr. Nancy Chesser
Dr. Arthur Lee
Ms. Marla Shain

Directed Technologies, Inc.
5945 Pacific Center Blvd.
Suite 510
San Diego, CA 92121
Attn: Dr. Robert A. Jacobsen

Dr. Harald O. Dogliani
P. O. Box 503
Los Alamos, NM 87544

C. S. Draper Laboratories
555 Technology Square
Cambridge, Massachusetts 02139
Attn: Dr. E. Olsson

ESL, Inc.
Mail Stop M-4216
495 Java Drive
Sunnyvale, CA 94088
Attn: Dr. Robert A. Marth

FM Technologies, Inc.
10529B Braddock Road
Fairfax, VA 22032
Attn: Dr. F. M. Mako

GA Technologies, Inc.
P. O. Box 85608
Code 02/503
San Diego, CA 93138
Attn: Dr. Vincent Chen
Dr. Hiroyuki Ikez

General Dynamics Corporation
1745 Jefferson Davis Highway
Suite 1000
Arlington, VA 22202
Attn: Dr. Daniel W. Roth

General Dynamics Corporation
Pomona Division
1675 W. Mission Blvd.
P. O. Box 2507
Pomona, CA 92769-2507
Attn: Dr. Ken W. Hawko
Mr. C. L. Featherstone

Grumman Corporation
Grumman Aerospace Research Ctr.
Bethpage, NY 11714-3580
Attn: Dr. Richard G. Madonna

Headquarters, Department of Army
DAMOFDE, Room 2D547
The Pentagon
Washington, DC 20310-0460
Attn: LTCOL Lou Goldberg

HQ Foreign Technology Division
Wright-Patterson AFB, OH 45433
Attn: TUTD/Dr. C. Joseph Butler

HQ USAF/TXN
Patrick Air Force Base, FL 32925
Attn: CAPT Joseph Nicholas

Hudson Institute
Center for Naval Analyses
Alexandria, VA 22302
Attn: Dr. F. Bomse

Hy-Tech Research Corp.
P. O. Box 3422 FSS
Radford, VA 24143
Attn: Dr. Edward Yadlowsky

Idaho Engineering National Lab.
P. O. Box 1625
Idaho Falls, ID 83415
Attn: Dr. Francis Tsang

Institute for Defense Analyses
1801 N. Beauregard Street
Alexandria, VA 22311
Attn: Dr. Deborah Levin
Ms. M. Smith

IRT Corporation
3030 Callan Road
San Diego, CA 92121
Attn: Dr. David Phelps

JAYCOR
11011 Torreyana Road
P. O. Box 85154
San Diego, CA 92138-9259
Attn: Dr. Franklin S. Felber
Dr. Seung Kai Wong

JAYCOR
39650 Libery Street, Suite 320
Freemont, CA 94538
Attn: Dr. Kendal Casey

Joint Institute for Laboratory
Astrophysics
National Bureau of Standards and
University of Colorado
Boulder, CO 80309
Attn: Dr. Arthur V. Phelps

Kaman Sciences
P. O. Draver QQ
Santa Barbara, CA 93102
Attn: Dr. W. Hobbs

La Jolla Institute
P. O. Box 1434
La Jolla, CA 92038
Attn: Dr. K. Brueckner

Lawrence Berkeley Laboratory
University of California
Berkeley, CA 94720
Attn: Dr. Edward P. Lee
Dr. Thomas Fessenden
Dr. William Fawley
Dr. Roger Bangerter

Lawrence Livermore National Laboratory
University of California
Livermore, California 94550
Attn: Mr. Arthur G. Cole
Dr. Michael Delong
MAJ Kenneth Dreyer
Dr. Ed Farley
Dr. Alex Glass
Dr. George Craig
Dr. C. V. Johnson, III
Dr. George Kamin
Dr. V. Kelvin Neil
Dr. Arthur C. Paul
Mr. Louis Reginato
Mr. Doyle Rogers
Dr. Dennis R. Slaughter
Dr. David Whittum
Dr. Simon S. Yu
Dr. Frank Chambers
Dr. James W.-K. Mark, L-477
Dr. William Barletta
Dr. William Sharp
Dr. John K. Boyd
Dr. John Clark
Dr. George J. Caporaso
Dr. Donald Prosnitz
Dr. John Stewart
Dr. Y. P. Chong
Dr. Hans Kruger
Dr. Thaddeus J. Orzechowski
Dr. John T. Weir
Dr. Yu-Jiuan Chen

Dr. James E. Leiss
13013 Chestnut Oak Drive
Gaithersburg, MD 20878

Lockheed Missiles and Space Co.
3251 Hanover St.
Bldg. 205, Dept 92-20
Palo Alto, CA 94304
Attn: Dr. John Siambis

Los Alamos National Laboratory
P.O. Box 1663
Los Alamos, NM 87545
Attn: Dr. L. Thode
Dr. H. Dogliani, MS-5000
Mr. R. Carlson, MS-P940
Dr. Carl Ekdahl, MS-D410
Dr. Joseph Mack
Dr. Melvin I. Buchwald
Dr. David C. Moir
Dr. Daniel S. Prono
Dr. S. Czuchlewski
Dr. Thomas P. Starke
Dr. Donald D. Cobb, D466
Dr. Robert R. Karl, D466
Dr. William B. Maier
Dr. John P. Rink
Dr. David Chamberlin

Maxwell Laboratories Inc.
8888 Balboa Avenue
San Diego, CA 92123
Attn: Dr. Ken Whitham
Dr. S. Echouse

McDonnell Douglas Research Laboratories
Dept. 223, Bldg. 33, Level 45
Box 516
St. Louis, MO 63166
Attn: Dr. Carl Leader
Dr. Frank Bieniosek
Dr. John Honig

Mission Research Corporation
1720 Randolph Road, S.E.
Albuquerque, NM 87106
Attn: Dr. Thomas Hughes
Dr. Lawrence Wright
Dr. Kenneth Struve
Dr. Michael Mostrom
Dr. Dale Welch

Mission Research Corporation
P. O. Drawer 719
Santa Barbara, California 93102
Attn: Dr. C. Longmire
Dr. N. Carron

Mission Research Corporation
8560 Cinderbed Road
Suite 700
Newington, VA 22122
Attn: Dr. Khanh Nguyen

National Inst. of Standards & Tech.
Gaithersburg, Maryland 20760
Attn: Dr. Mark Wilson

National Inst. of Standards & Tech.
Radiation Physics Bldg. Room C229
Washington, DC 20234
Attn: Dr. Wayne Cassatt

National Security Agency
4928 College Avenue
College Park, MD 20740
Attn: Dr. Albert J. Leyendecker

Naval Ocean Systems Center
San Diego, CA 92152
Attn: CAPT James Fontana
Mrs. Teresita Finch
Dr. Rodney Buntzen

Naval Postgraduate School
Physics Department (Code 61)
Monterey, CA 93940
Attn: Prof. John R. Neighbours
Prof. Fred Buskirk
Prof. Kai Woehler
Prof. Xavier Maruyama

Naval Surface Warfare Center
Dahlgren, VA 22448-5000
Attn: Dr. E. M. Williams
Mr. C. E. Gallaher
Mr. Lawrence Luessen
Ms. Theresa Houghton
Dr. Ronald J. Gripshover
Dr. S. L. Moran
Dr. Edwin Ball

Naval Surface Warfare Center
White Oak Laboratory
Code R-41
Silver Spring, Maryland 20903-5000
Attn: CAPT R. P. Fuscaldo
Dr. Thomas A. Clare
CAPT R. W. Moore
Dr. Ira Blatstein
Mr. Kenneth Caudle
Mr. Carl Larson
Dr. Robert DeWitt
Dr. Ralph Schneider
Dr. Joel Miller
Dr. Stanley Stern
Dr. Omer Goktepe
Dr. A. L. Licht
Dr. Joon Choe
Mr. David Demske
Dr. Jag Sharma
Mr. W. M. Hinckley
Dr. H. S. Uhm
Dr. R. Fiorito
Dr. R. Stark
Dr. H. C. Chen
Dr. D. Rule
Dr. Matt Brown
Mrs. Carolyn Fisher (G42)
Dr. Eugene E. Nolting (H23)

Naval Technical Intelligence Center
Code DA52
4301 Suitland Road
Washington, DC 20395
Attn: Mr. Mark Chapman

New Mexico State University
Research Center
Box RC
Las Cruces, NM 88003-0001
Attn: Dr. Leon J. Radziemski

Northeastern University
Dept. of Elec. Engineering
360 Huntington Avenue
Boston, MA 02115
Attn: Dr. Philip Serafim

North Star Research Corp.
5555 Zuni, S. E.
Albuquerque, NM 87104
Attn: Dr. Richard Adler

Oak Ridge National Laboratory
Health & Safety Research Div.
P. O. Box X
Oak Ridge, TN 37830
Attn: Dr. Rufus H. Ritchie
Dr. O. Crawford

Office of the Chief of Naval Operation
Strategic and Theatre Nuclear Warfare
OP-654E4
The Pentagon
Washington, DC 20350
Attn: Dr. Yong S. Park

Office of Naval Research
800 North Quincy Street
Arlington, VA 22217
Attn: Dr. C. W. Roberson
Dr. F. Saalfeld

Office of Naval Research (2 copies)
Department of the Navy
Code 01231C
Arlington, VA 22217

Office of Under Secretary of Defense
Research and Engineering
Room 3E1034
The Pentagon
Washington, DC 20301
Attn: Dr. John MacCallum

OSWR
P. O. Box 1925
Washington, DC 20013
Attn: Dr. Jose F. Pina

PhotoMetrics, Inc.
4 Arrow Drive
Woburn, MA 01801
Attn: Dr. Irving Kofsky

Physics International, Inc.
2700 Merced Street
San Leandro, CA. 94577
Attn: Dr. E. Goldman
Dr. James Benford
Dr. George B. Frazier
Mr. Ralph Genuario

Princeton University
Plasma Physics Laboratory
Princeton, NJ 08540
Attn: Dr. Francis Perkins, Jr.

Pulse Sciences, Inc.
600 McCormack Street
San Leandro, CA 94577
Attn: Dr. Sidney Putnam
Dr. Vernon Bailey
Dr. M. Tiefenbach
Dr. J. Edighoffer
Mr. James Fockler

Pulse Sciences, Inc.
2001 Wilshire Boulevard
Suite 600
Santa Monica, CA 90403
Attn: Dr. John R. Bayless

R&D Associates
301A South West Street
Alexandria, VA 22314
Attn: Mr. Ihor Vitkovitsky
Dr. Peter Turchi

The Rand Corporation
2100 M Street, NW
Washington, DC 20037
Attn: Dr. Nikita Wells
Mr. Simon Kassel

Sandia National Laboratory
Albuquerque, NM 87115
Attn: Dr. Collins Clark
Dr. John Freeman/1241
Dr. Charles Frost
Dr. Gerald N. Hays
Dr. Michael G. Mazarakis/1272
Dr. John Wagner/1241
Dr. Ron Lipinski/1274
Dr. James Poukey
Dr. Milton J. Clauser/1261
Dr. Kenneth R. Prestwich/1240
Dr. Kevin O'Brien
Dr. Isaac R. Shokair
Dr. J. Pace VanDevender/1200
Dr. J. T. Crow
Dr. S. Shope
Dr. B. N. Turman
Dr. C. Olson
Dr. Richard Adams
Dr. Malcolm Buttram
Mr. Charles Crist
Dr. Susan Fisher
Dr. John Keizur
Dr. Gordon T. Leifeste
Dr. Raymond W. Lemke
Dr. Juan Ramirez
Dr. James Rice
Dr. Michael Wilson

Science Applications Intl. Corp.
2109 Air Park Road, S. E.
Albuquerque, NM 87106
Attn: Dr. R. Richardson
Dr. Michael D. Haworth
Dr. Alan J. Toepfer

Science Applications Intl Corp.
5150 El Camino Road
Los Altos, CA 94022
Attn: Dr. R. R. Johnston
Dr. Leon Feinstein
Dr. Douglas Keeley
Dr. E. Roland Parkinson

Science Applications Intl. Corp.
1710 Goodridge Drive
McLean, VA 22102
Attn: Mr. W. Chadsey
Dr. A Drobot
Dr. K. Papadopoulos
Dr. William W. Rienstra
Dr. Alfred Mondelli
Dr. D. Chernin
Dr. R. Tsang
Dr. J. Petillo
Dr. G. Bourianoff
Ms. K. Wilson

Science Research Laboratory, Inc.
1600 Wilson Boulevard
Suite 1200
Arlington, VA 22209
Attn: Dr. Joseph Mangano
Dr. Daniel Birx

Commander
Space & Naval Warfare Systems Command
PMW-145
Washington, DC 20363-5100
Attn: CDR W. Fritchie
Mr. D. Merritt

Space Power Institute
315 Leach Science Center
Auburn University
Auburn, AL 36845-3501
Attn: Prof. M. Frank Rose

Spectra Technology
2755 Northup Way
Bellevue, WA 98004
Attn: Dr. Dennis Loventhal
Dr. Steve Baughoum
Dr. James Ewing

SRI International
PS0-15
Molecular Physics Laboratory
333 Ravenswood Avenue
Menlo Park, CA 94025
Attn: Dr. Donald Eckstrom
Dr. Kenneth R. Stalder
Dr. Roberta Saxon
Dr. Jay Dickerson

Strategic Defense Initiative Org.
SDIO/T/DE0
The Pentagon
Washington, DC 20301-7100
Attn: COL Thomas Meyer (DEWO)
LTC Michael toole (DEWO)
MAJ J. Wills
Dr. Dwight Duston
LTC Ed Pogue
Dr. Kevin Probst
Dr. Charles Sharn

System Planning Corporation
1500 Wilson Boulevard, Room 1213W
Arlington, VA 22209
Attn: Mr. James T. Lacatski

Titan/Spectron, Inc.
P. O. Box 4399
Albuquerque, NM 87196
Attn: Dr. R. Bruce Miller
Dr. John Smith

Titan Systems, Inc.
5910 Pacific Center Blvd.
San Diego, CA 92121
Attn: Dr. R. M. Dowe, Jr.

Tetra Corporation
4905 Hawkins Street, N. E.
Albuquerque, NM 87109-4345
Attn: Mr. William Money

University of California
Physics Department
Irvine, CA 92664
Attn: Dr. Gregory Benford
Dr. Norman Rostoker

University of California
San Diego, CA 92110
Attn: Dr. Marshall N. Rosenbluth

UCLA
Physics Department
Los Angeles, CA 90024
Attn: Dr. F. Chen
Dr. C. Joshi
Dr. J. Dawson
Dr. N. Luhmann
Dr. W. Barletta
Dr. T. Katsouleas

University of Colorado
Dept. of Astrophysical, Planetary
& Atmospheric Sciences
Boulder, CO 80309
Attn: Dr. Scott Robertson

University of Illinois at Chicago
Dept. of Physics
P. O. Box 4348
Chicago, IL 60680
Attn: Dr. Charles K. Rhodes

University of Maryland
College Park, MD 20742
Attn: Dr. J. Goldhar
Dr. W. Destler
Dr. C. Striffler
Dr.Moon-Jhong Rhee

University of Michigan
Dept. of Nuclear Engineering
Ann Arbor, MI 48109
Attn: Prof. Terry Kammash
Prof. R. Gilgenbach

University of New Mexico
Dept. of Chem. & Nuclear Engineering
Albuquerque, NM 87131
Attn: Prof. Stanley Humphries

Commander
U. S. Army Laboratory Command
2800 Powder Mill Road
Adelphi, MD 20783-1145
Attn: George Albrecht (AMSLC-TP-PL)

U. S. Army Combined Army Center
ATZL-CAG
Ft. Leavenworth, KS 68027-5000
Attn: LTC Orville Stokes

Yale University
Mason Laboratory
New Haven, CN 06520
Attn: Dr. Ira Bernstein

Director of Research
U.S. Naval Academy
Annapolis, MD 21402 (2 copies)